doi:10.1038/nature11703

S1. Model parameters

Figure S1 and Table S1 show the model geometry and parameters used in the simulation presented in the main article.

S2. Model response that reproduces a range of observations

The rich model response described in the main text is animated by the two supplementary movies which show the time evolution of slip rate distribution $V_z(x, z, t)$ on the fault from 4300 to 4800 years (movie I) and from 3500 to 4000 years (movie II) after the beginning of the numerical simulation. Coseismic slip rates of the order of 0.1 m/s and higher are indicated by white to blue colors. The slower slip rates are shown in progressively darker yellow and orange, with the long-term plate rate of 10^{-9} m/s indicated in red. Locked regions which have, by definition, much smaller slip rates than the plate rate are indicated by black patches. The simulated time and the maximum slip rate over the fault at that time are given at upper-right and upper-left corners of the movies, respectively. The movie frames are taken every 30 computational time steps, which vary in the computation, and hence the time intervals between the frames are quite heterogeneous. During coseismic periods, the typical time step is 2/150 s and the typical interframe rate is 0.4 s. In the interseismic periods, the interframe rates reach values of about 1 year.

Movie I illustrates the behavior of the model that combines, in the same patch, creep in the interseismic periods and large seismic slip. It starts at a time when the interseismic fault slip rate distribution is as expected for the slow-rate friction properties adopted in the model: patch A is mostly locked and patch B is creeping with the long-term plate rate, like the creeping areas that surround the two patches. During the following interseismic period, the locked region of patch A shrinks by penetration of creep from the surrounding areas, which occurs due to stress concentration at the boundary between creeping and locked regions (e.g., Tse and Rice, 1986; Lapusta et al., 2000). Earthquake rupture nucleates when the creeping region within patch A becomes comparable to the nucleation size estimates (Rice and Ruina, 1983; Rice et al., 2001; Rubin and

Ampuero, 2005; Chen and Lapusta, 2009), In movie I, this occurs for the first time at 4340 years, in the bottom-left corner of patch A. Earthquake rupture propagates in a complex manner, rupturing the steadily-creeping patch B and then re-rupturing patch A. Right after the event, both patches combine to form one locked region, with the surrounding areas experiencing accelerated postseismic slip, amply documented in observations (Hsu et al., 2006; Bruhat et al., 2011; Ozawa et al., 2011). The subsequent fault behavior features two smaller earthquakes, at 4432 and 4589 years, which nucleate in and rupture patch A but fail to rupture patch B. The first of these events arrests in patch B while the patch is partially locked, while the second one arrests in patch B while it is fully creeping. Then, rupture nucleates close to the middle of the fault, in top-right corner of patch A, and ruptures into patch A first, then penetrating into (creeping) patch B, growing there, and partially re-rupturing patch A. This is the event that is used for Figure 3 of the main text. Note that such rerupturing was inferred for the 2011 Tohoku-Oki earthquake (Ide et al., 2011; Lee et al., 2011 GRL). After the event, the area of seismic slip again appears mostly locked, with the surrounding areas experiencing postseismic slip.

Movie II illustrates a 500-year long time period in the model history when patch B remains at least partially locked at all times, even before model-spanning events. This is because shear stress in the middle of that patch stays below the level needed for creep with the plate rate. Conventional interpretation would treat this region as the one with rate-weakening rate-and-state properties, since it remains locked in the interseismic period. Yet, this region has rate-strengthening properties at low slip rates, and exhibits such behavior due to the combination of coseismic weakening and slip history of the fault. Indeed, as movie I shows, the same region can be fully creeping with the long-term plate rate at other times in the same model.

Note that the seismic rupture can arrest in or propagate through patch B when the patch is either creeping or partially locked. So one cannot make conclusions on whether the event will or will not arrest in patch B based on whether it is locked or creeping. In particular, the smaller event at 4432 years arrests in the middle of a locked segment, which would be puzzling based on the observations of slip alone. However, this is not at all surprising given the physics of patch B, which is rate-strengthening until the coseismic weakening is activated, and hence can have quite high resistance to seismic slip.

In the interseismic periods, both patches find themselves locked after seismic slip and then experience penetration of creeping fronts from the surrounding creeping areas. However, the creep-in process occurs differently in the two patches. In patch A, it produces spontaneous aseismic transients, which have been observed in previous studies (Liu and Rice, 2005; Lapusta and Liu, 2009). These transients are part of the nucleation processes on rate-weakening faults and they are enhanced in models with the aging law (Rubin, 2008) and for conditions that favor large nucleation sizes, such as low effective normal stress (Liu and Rice, 2005). In this model, their spatial extent is enhanced by the transition region of 10-km width between the patch A and the surrounding area, in which the value of the nucleation size is larger than that in patch A. Patch B is rate-strengthening at low slip rates and thus unable to produce aseismic transients or earthquake nucleation. Hence the creep-in process in patch B occurs steadily and without transients. Note that more complex behavior may result in rate-strengthening regions with heterogeneous properties (Perfettini and Ampuero, 2008).

Shear stress as a function of slip at representative points of patches A and B located at $(x, z) = (-24$ km, 0 km) and (24 km, 0 km), respectively, is plotted in Figure S2a. When patch B slips coseismically (Figure S2b), gradual weakening with meters of the apparent slip weakening distance follows sharper decrease in the shear stress due to state evolution. As already discussed, patch B can also creep steadily with the nearly-constant shear stress. Figure S3 gives slip and slip rate as functions of time at the same points as in Figure S2. The recurrence time of seismic slip is clearly different between the two patches. It is again clear that Patch B sometimes creeps at slip rates near the plate rate which is indicated by a horizontal dashed line in Figure S3b.

S3. Activation of coseismic weakening in the patch with rate-strengthening at low slip rate

Dynamic rupture enters patch B due to stress concentration at the rupture front. Whether the rupture can continue and grow in patch B depends on whether it manages to activate coseismic weakening. Before such activation, rate-strengthening properties result in increasing resistance for higher (seismic) slip rates, effectively causing negative dynamic stress drop locally. However, rupture can penetrate into a region of negative stress drop due to wave-induced stress concentration at its front, although it would be losing energy in such regions. If such a rupture succeeds in activating coseismic weakening such as thermal pressurization,

starting to produce positive dynamic stress drop and feeding itself with large enough energy release rate, then the rupture can recover and even start growing.

Thus, the process of activating coseismic weakening in patch B depends on a number of factors, including properties of patch B, the characteristics of the incoming rupture, and the prestress/state of patch B right before the event. Patch B is more susceptible to thermal pressurization (e.g., the coseismic weakening is activated there over smaller slips) if it has higher degree of shear localization (e.g., a smaller width w of the shear layer), smaller hydraulic permeability and storage capacity, and a higher reference friction coefficient. The incoming rupture penetrates deeper into patch B if its tip has a large region of higher stress concentration in front, which is promoted by larger dynamic stress drop and longer rupture propagation. Larger prestress and smaller values of the state variable (that determines the degree of healing) in patch B would also favor rupture penetration into patch B. Note that, initially, the rupture does not need to penetrate into patch B over the entire width of the fault; it can activate coseismic weakening only in a portion of it, and the resulting rapidly increasing rupture would concentrate stress on the nearby regions, aiding in activating coseismic weakening there.

Overall, the importance of many factors, some of which definitely vary with time (e.g., the size of the incoming event), implies that even rate-strengthening regions that are in principle susceptible to coseismic weakening may not be ruptured in several seismic events before succumbing to a larger and/or well-positioned event. The response of our model illustrates that. The cases of seismic events being arrested by large creeping regions are well-documented, for example, the 2004 Parkfield earthquake (e.g., Johanson et al., 2006), the 2005 Nias earthquake (Hsu et al., 2006), and the 2007 Pisco earthquake (Perfettini et al. 2007). This may imply that, in those areas, the creeping regions are not susceptible to coseismic weakening. Or it may be because the events were not energetic enough, and the creeping areas may be ruptured in the future by larger incoming events. Often, we do not have observational constraints on whether a given area was locked or creeping before an earthquake. As observational evidence accumulates, it will become clearer whether co-seismic rupturing of creeping segments occurs on natural faults and how frequently. Meanwhile, more numerical and experimental studies are needed to achieve a quantitative theoretical understanding of this problem.

Let us estimate slip δ_{drop} required for the rupture to start producing positive dynamic stress drops in patch B. Let us assume that patch B is creeping with the long-term plate rate, and hence has the shear stress $\tau_{ini} = \sigma_{e0}[f_{0B} + (a - b_B)\log(V_{pl} / V_0)]$. (The variables are defined in the "Methods" section.) The shear stress due to higher friction at seismic slip rates V_{seis} can be estimated as $\tau_{seis} = \sigma_{e0}[f_{0B} + (a - b_B)\log(V_{seis} / V_0)]$, with the resulting strengthening of $\Delta\tau_{str} = \sigma_{e0}(a - b_B)\log(V_{seis}/V_0)$. Note that, due to the direct effect and subsequent state variable evolution, the stress would first increase to values higher than τ_{seis} and then evolve to τ_{seis}, but this will occur over much smaller slips as shown in Figure S2 and discussed later. The slip δ_{half} required for reducing the effective normal stress twice due to thermal pressurization (and hence getting to stress levels of $\tau_{seis} / 2$) can be estimated either for the case of slip on a mathematical plane (L^* from equation (23) of Rice, 2006) or for the adiabatic and undrained limit (equation (16) of Rice, 2006); these estimates for V_{seis} = 1 m/s and properties of patch B are 1.86 m and 1.45 m, respectively. Then, making an assumption of a constant weakening rate (which is not exact but can give us an order of magnitude estimate), we get:

$$\frac{\tau_{seis} / 2}{\delta_{half}} = \frac{\Delta\tau_{str}}{\delta_{drop}} \text{ or } \delta_{drop} = \delta_{half}\frac{\Delta\tau_{str}}{\tau_{seis} / 2} = 0.364\delta_{half}, \quad \text{(S1)}$$

which results in δ_{drop} of about 0.5-0.7 m for V_{seis} = 1 m/s and properties of patch B.

These estimates suggest that coseismic slip of the order of 0.1 to 1 m in patch B is large enough to start producing positive dynamic stress drop in our model. Whether such a condition is met for any given rupture, enabling its propagation in patch B, is dictated by many factors including the location of nucleation and the amount of stress transferred by the rupture of patch A onto patch B through radiated waves. Those complexities are shown in the supplementary movies.

S4. Comparison with the model by Noda and Lapusta (2010)

Noda and Lapusta (2010) presented simulations in a model with two smaller patches of identical rate-weakening frictional properties ($a - b < 0$) (Figure S4a). (The patches in the model of the main text are larger to reflect the size of the Chi-Chi earthquake source.) The frictional properties used in Noda and Lapusta (2010) are listed in Table S2. To determine the effect of the rate-strengthening vs. rate-weakening behavior in patch B, we have conducted simulations like in Noda and Lapusta (2010) but with rate-strengthening in patch B; $a - b_B = -0.004$ in the model by Noda and Lapusta (2010) and 0.004 in the supplementary simulation presented here.

Figures S4b and c show cumulative slip at the mid-depth for positive and negative $a - b_B$, respectively. There are remarkable similarities in the patterns of earthquakes. The model-spanning events nucleate in patch A, have larger slip in patch B, and occasionally generate backward rupture propagation from patch B to A (Noda and Lapusta, 2010). There are smaller and more frequent events which rupture only patch A. However, the recurrence time of the mode-spanning events are longer in the model with the positive ($a - b_B$). The interseismic coupling ratio also shows significant difference between the two cases (Figures S4d and e). In the case with positive $a - b_B$, patch B is much more prone to creep compared with the case with negative $a - b_B$. As the result, the distribution of the coupling ratio just before model-spanning events varies from one earthquake to another in the case of patch B with positive $a - b_B$, similarly to the model presented in the main text.

The coseismic fault behavior of patch B in model-spanning events is also significantly affected by the rate-strengthening properties. Figures S5a and b represent snapshots of slip rate distribution along the mid-depth of the fault for the cases with positive and negative $a - b_B$, respectively, during model-spanning events indicated by yellow color in Figures S4b and c. With positive $a - b_B$, the peak in the slip rate at the rupture front is smoother, similar to the model presented in the main body, compared to the sharp peak at the rupture front with negative $a - b_B$. Figures S5c and d indicate the spectral structure of the source-time functions in representative points in patch A and B for the same events. In both cases, patch B has larger slip and thus larger amplitude in low frequency than patch A. In the case with negative $a - b_B$ (Figure S5d), the power spectrum decays more rapidly in patch B than in patch A, showing the effect of more gradual weakening due to thermal pressurization noticed by Andrews (2005). In the case of positive $a - b_B$, however, the power

spectrum in patch B decreases even more rapidly with frequencies (Figure S5c), similarly to the model in the main text, resulting in lower high-frequency amplitudes than in patch A. In this supplementary case, which is studied for comparison with Noda and Lapusta (2010), the depletion occurs at frequencies higher than can be typically observed. The study of the range of rate-and-state and poroelastic parameters that would result in the frequency depletion at different observable frequency bands is an important goal of future work.

References

Andrews, D. J. (2005), Thermal pressurization explains enhanced long-period motion in the Chi-Chi earthquake, Eos Trans. AGU, 86(52), Fall Meet. Suppl., Abstract S34A‐04.

Bruhat, L., S. Barbot, and J.P. Avouac (2011), Evidence for postseismic deformation of the lower crust following the 2004 Mw6.0 Parkfield earthquake, J. Geophys. Res., 116, B08401, doi:10.1029/2010JB008073.

Chen, T., and N. Lapusta (2009), Scaling of small repeating earthquakes explained by interaction of seismic and aseismic slip in a rate and state fault model, J. Geophys. Res., 114, B01311, doi:10.1029/2008JB005749.

Hsu, Y.J., M. Simons, J.P. Avouac, J. Galetzka, K. Sieh, M. Chlieh, D. Natawidjaja, L. Prawirodirdjo, and Y. Bock (2006), Frictional afterslip following the 2005 Nias-Simeulue earthquake, Sumatra, Science, 312, 1921-1926.

Ide, S., A. Baltay, and G. C. Beroza (2011) Shallow dynamic overshoot and energetic deep rupture in the 2011 Mw 9.0 Tohoku-Oki earthquake, Science, 332, 1426–1429, doi:10.1126/science.1207020.

Johanson, I. A., E. J. Fielding, F. Rolandone, R. Burgmann (2006), Coseismic and postseismic slip of the 2004 Parkfield earthquake from space-geodetic data, Bull. Seismol. Soc. Am., 96, S269–S282.

Lapusta, N., and Y. Liu (2009), Three‐dimensional boundary integral modeling of spontaneous earthquake sequences and aseismic slip, J. Geophys. Res., 114, B09303, doi:10.1029/2008JB005934.

Lapusta, N., J. R. Rice, Y. Ben‐Zion, and G. Zheng (2000), Elastodynamic analysis for slow tectonic loading with spontaneous rupture episodes on faults with rate- and state-dependent friction, J. Geophys. Res., 105(B10), 23,765–23,789, doi:10.1029/2000JB900250.

Lee, S.J., B.S. Huang, M. Ando, H.C. Chiu, and J.H. Wang (2011), Evidence of large scale repeating slip during the 2011 Tohoku-Oki earthquake, Geophys. Res. Lett., 38, L19306, doi:10.1029/2011GL049580

Liu, T., and J. R. Rice (2005), Aseismic slip transients emerge spontaneously in 3D rate and state modeling of subduction earthquake sequences, J. Geophys. Res., 110, B08307, doi:10.1029/2004JB003424.

Noda H., and N. Lapusta (2010), 3D earthquake sequence simulations with evolving temperature and pore pressure due to shear heating: Effect of heterogeneous hydraulic diffusivity, J. Geophys. Res., 115, B12314,doi:10.1029/2010JB007780.

Ozawa, S., T. Nishimura, H., Suito, T. Kobayashi, M. Tobita, and T. Imakiire (2011), Coseismic and postseismic slip of the 2011 magnitude-9 Tohoku-Oki earthquake, Nature, 475, 373-376, doi10.1038/nature10227.

Perfettini, H., J.P. Avouac, H. Tavera, A. Kositsky, J.M. Nocquet, F. Bondoux, M. Chlieh, A. Sladen, L. Audin, D. L. Farber, P. Soler (2007), Seismic and aseismic slip on the Central Peru megathrust, Nature, 465, 78–81, doi:10.1038/nature09062.

Perfettini, H., and J.-P. Ampuero (2008), Dynamics of a velocity strenghtening region: implications for slow earthquakes and postseismic slip J. Geophys. Res., 113 (B9), B09411, doi:10.1029/2007JB005398

Rice, J. R. (2006), Heating and weakening of faults during earthquake slip, J. Geophys. Res., 111, B05311, doi:10.1029/2005JB004006.

Rice, J. R., N. Lapusta, and K. Ranjith (2001), Rate and state dependent friction and the stability of sliding between elastically deformable solids, J. Mech. Phys. Solids, 49, 1865–1898, doi:10.1016/S0022-5096(01)00042-4.

Rubin, A. M. and Ampuero, J.-P. (2005). Earthquake nucleation on (aging) rate and state faults, J. Geophys. Res., 110, B11312. doi:10.1029/2005JB003686.

Rubin, A. M. (2008), Episodic slow slip events and rate-and-state friction, J. Geophys. Res., 113, B11414, doi:10.1029/2008JB005642.

Tanikawa, W., T. Shimamoto, S. K. Wey, C. W. Lin, and W. C. Lai (2008), Stratigraphic variation of transport properties and overpressure development in the Western Foothills, Taiwan, J. Geophys. Res., 113, B12403, doi:10.1029/2008JB005647.

Elastodynamics					
S-wave speed	c_s	3000 m/s			
Shear modulus	μ	30 GPa			
Poisson's ratio	ν	0.25			
Frictional properties					
Reference slip rate *	V_0	1 μm/s			
Reference friction *	f_{0A}	0.7	f_{0B}	0.4	
Rate dependency *	$a - b_A$	−0.002	$a - b_B$	0.004	
Direct effect parameter **	a	0.0066			
State-evolution distance	L_{AB}	8 mm			
Hydrothermal properties					
Thermal diffusivity	α_{th}	10^{-6} m^2/s			
Hydraulic diffusivity *	α_{hyA}	3.5×10^{-2} m^2/s	α_{hyB}	7.0×10^{-5} m^2/s	
Specific heat *	ρc	2 MPa/K			
Undrained $\partial p/\partial T$ *	Λ_A	0.036 MPa/K	Λ_B	0.069 MPa/K	
Shear-zone width	w_{AB}	8 mm			
Boundary conditions and geometry					
Plate velocity	V_{pl}	10^{-9} m/s			
Initial effective normal stress	σ_{e0}	60 MPa			
Patch size	$2W_1$	35 km			
Distance between patches	W_2-W_1	10 km			

Table S1. Model parameters used in the simulation presented in the main text. The values marked by * are taken from Tanikawa and Shimamoto (2009), with hydraulic properties corresponding to 60 MPa effective pressure. The values marked by ** are obtained from Tanikawa and Shimamoto, personal communication.

Elastodynamics					
S-wave speed	c_s	3000 m/s			
Shear modulus	μ	30 GPa			
Poisson's ratio	ν	0.25			
Frictional properties					
Reference slip rate	V_0	1 μm/s			
Reference friction	f_{0A}	0.6	f_{0B}	0.6	
Rate dependency	$a - b_A$	−0.004	$a - b_B$	$\pm$0.004	
Direct effect parameter	a	0.01			
State-evolution distance	L_{AB}	4 mm			
Hydrothermal properties					
Thermal diffusivity	α_{th}	10^{-6} m^2/s			
Hydraulic diffusivity	α_{hyA}	1×10^{-2} m^2/s	α_{hyB}	1×10^{-4} m^2/s	
Specific heat	ρc	2.7 MPa/K			
Undrained $\partial p/\partial T$	Λ_A	0.1 MPa/K	Λ_B	0.1 MPa/K	
Shear zone width	w_{AB}	10 mm			
Boundary conditions and geometry					
Plate velocity	V_{pl}	10^{-9} m/s			
Initial effective normal stress	σ_{e0}	30 MPa			
Patch size	$2W_1$	15 km			
Distance between patches	W_2-W_1	5 km			

Table S2. Model parameters used in the simulation presented in Figures S4 and S5. The case with negative ($a - b$) is identical to the one in Noda and Lapusta (2010).

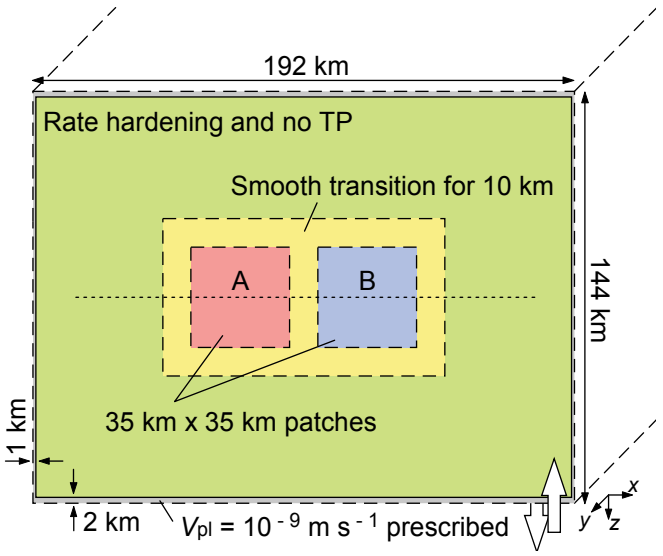

Figure S1. Geometry of the model presented in the main text. The size of the system is comparable to the source region of the 1999 ChiChi, Taiwan, earthquake.

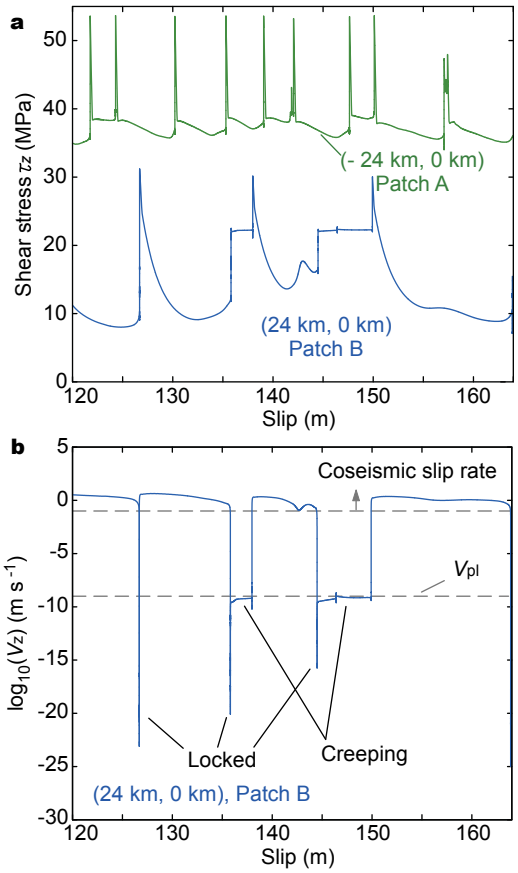

Figure S2. Evolution in shear stress and slip rate at representative fault points as a function of slip. (a) Shear stress in the loading (z) direction at representative points of patches A and B. During model-spanning events which cause coseismic slip in patch B, weakening is dominated by thermal pressurization which causes an apparently long weakening distance, as anticipated based on the study of Rice (2006). (b) Slip rate in the z-direction as a function of slip in patch B. Significant amount of slip is accommodated by creeping motion at a slip rate around the plate rate 10^{-9} m/s.

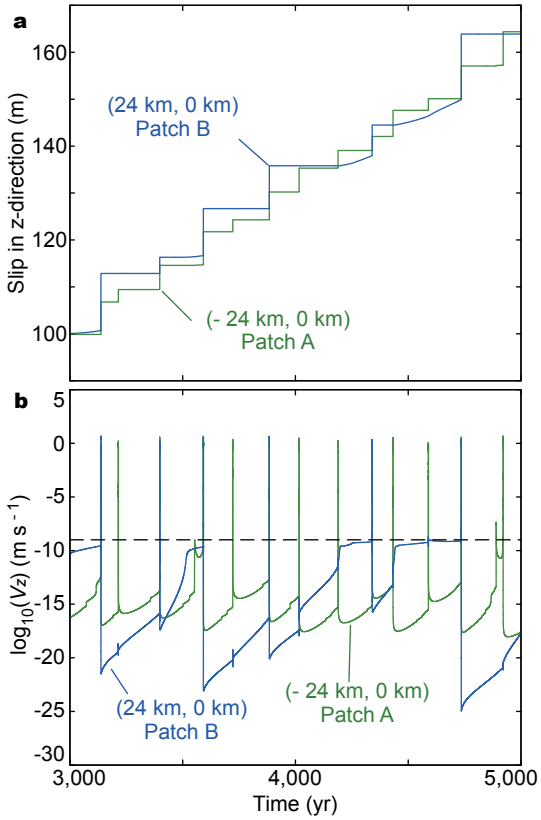

Figure S3. Evolution in shear stress and slip rate at representative points as a function of time. (a) Slip and (b) slip rate in the *z*-direction at the same two points as in Figure S2. Recurrence intervals are different in the two patches. Patch B (blue line) can stay near the plate rate (10^{-9} m/s) steadily for hundreds of years (e.g., between 4440 and 4740 years), waiting for rupture from patch A to give it a large enough kick to activate dynamic weakening and cause destructive coseismic slip there.

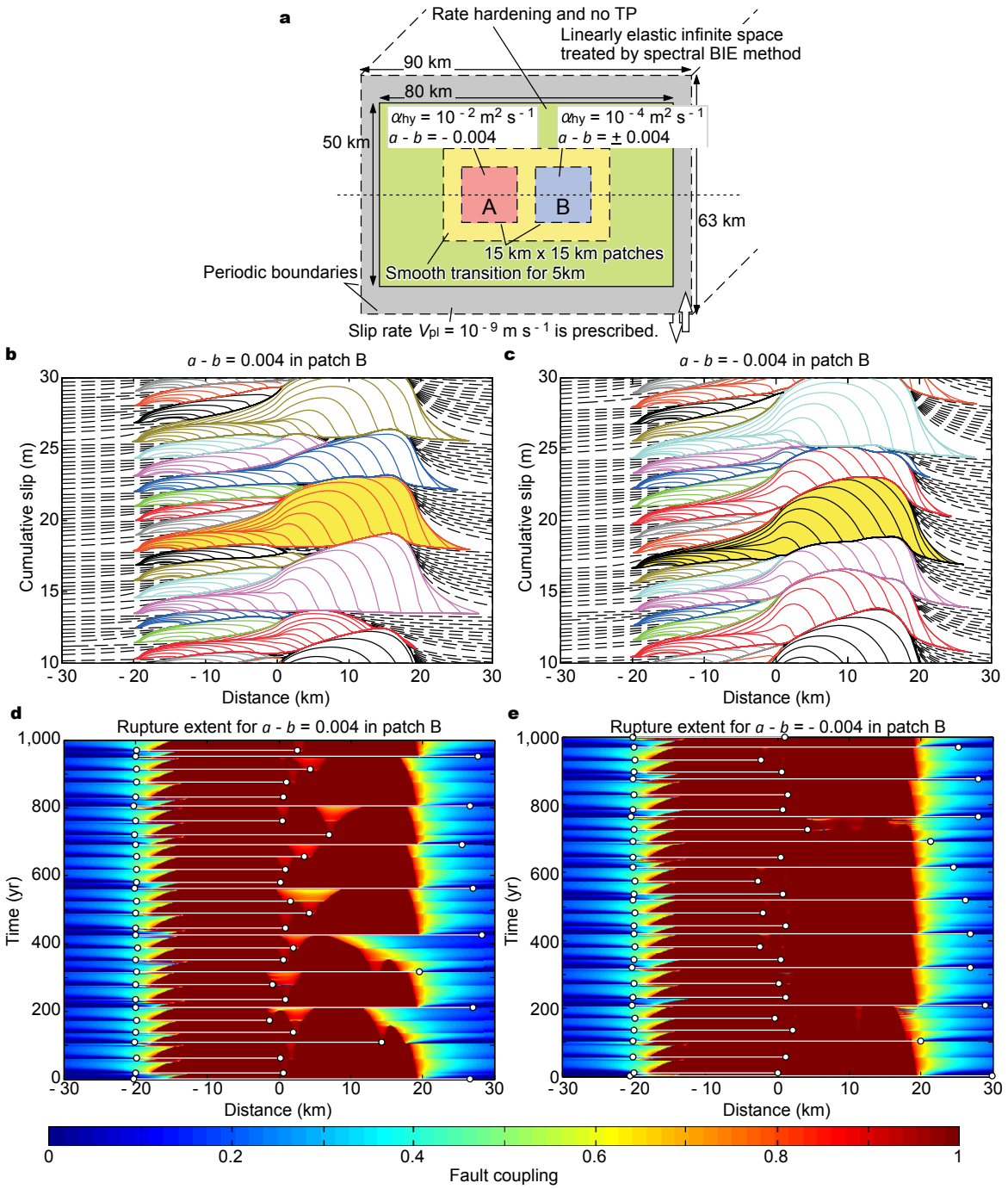

Figure S4. Comparison of the long-term behavior between the supplementary calculation and a model presented in Noda and Lapusta (2010). (a) Model setting used in Noda and Lapusta (2010). We use it to test the differences between positive and negative values of $(a - b_B)$. (b-c) Cumulative slip for models with positive (b) and negative (c) values of $(a - b_B)$. The overall pattern is similar in the two cases, but the model with positive $(a - b_B)$ has a longer recurrence time for the model-spanning events. (d-e) Coupling ratio for models with positive (d) and negative (e) $(a - b_B)$, showing clear differences in coupling in patch B in the two models. The ruptures are indicated by white lines with circles at their ends.

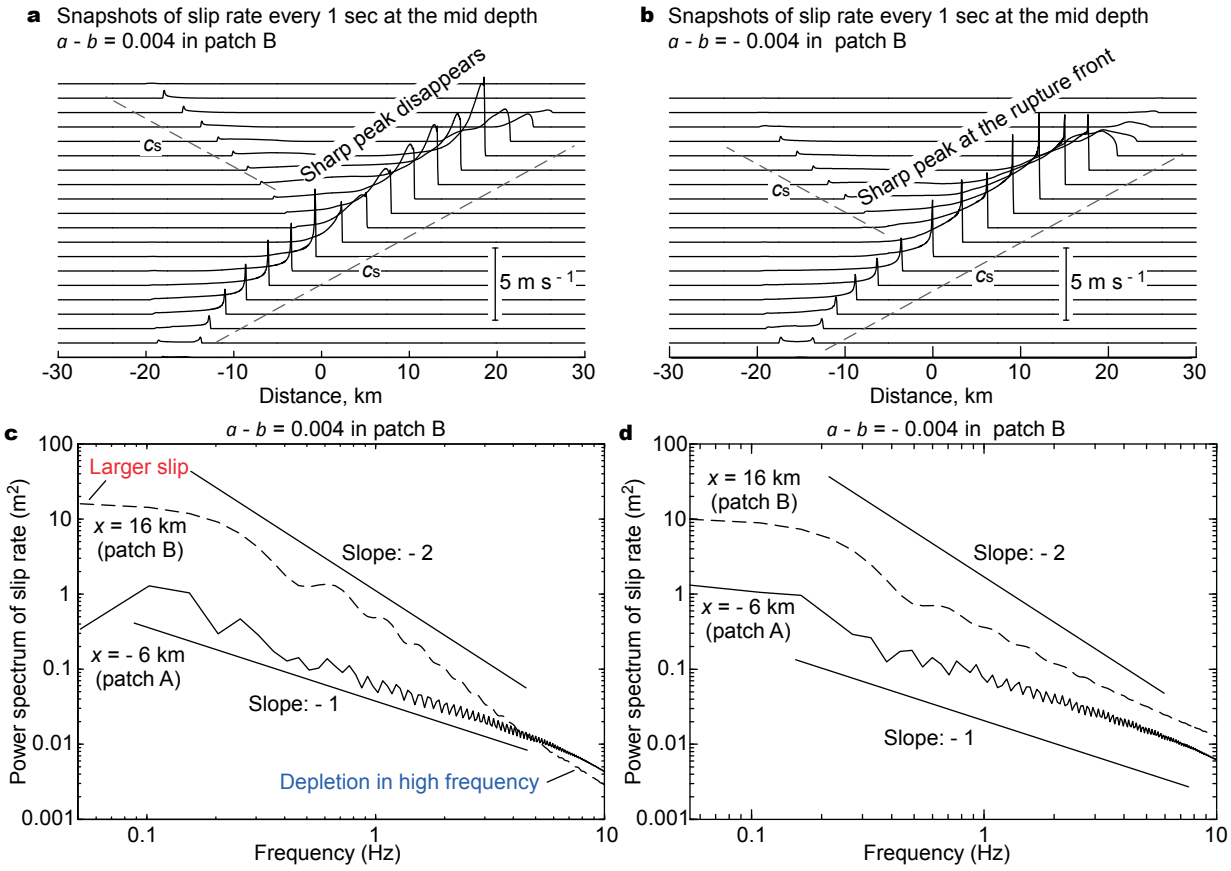

Figure S5. Comparison of the coseismic behavior between the supplementary calculation and a model presented in Noda and Lapusta (2010). (a-b) Snapshots of the slip-rate distribution along the mid-depth every 1 s during events indicated in Figure S4 (b) and (c) by yellow, respectively. We see that the case with rate strengthening in patch B has smoother slip-rate shapes there. (c-d) Power spectrum of the source-time function at $x = -6$ km (patch A) and 16 km (patch B), in the same events as in (a) and (b), respectively. In both cases, patch B has steeper fall off of high frequencies than patch A, due to larger slip weakening distances of thermal pore pressurization. The decay of the power spectrum with frequency in patch B is more pronounced in the case with rate-strengthening properties (c).